pubs.acs.org/ac

analytical chemistry

October 15, 2009 Volume 81 Number 20

In Situ Metabolic Profiling of Single Cells by Laser Ablation Electrospray Ionization Mass Spectrometry

Discrimination of Thioarsenites and Thioarsenates by X-ray Absorption Spectroscopy

Characterization of *Lapis Lazuli* Pigments Using a Multitechnique Analytical Approach

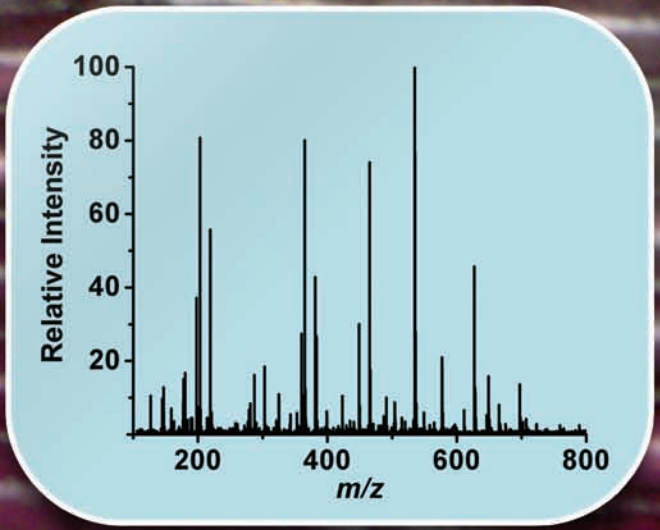

ACS Publications
High quality. High impact.

www.acs.org

Anal. Chem. **2009,** *81,* 8265–8271

Accelerated Articles

In Situ Metabolic Profiling of Single Cells by Laser Ablation Electrospray Ionization Mass Spectrometry

Bindesh Shrestha and Akos Vertes*

Department of Chemistry, W. M. Keck Institute for Proteomics Technology and Applications, The George Washington University, Washington, District of Columbia 20052

Depending on age, phase in the cell cycle, nutrition, and environmental factors, individual cells exhibit large metabolic diversity. To explore metabolic variations in cell populations, laser ablation electrospray ionization (LAESI) mass spectrometry (MS) was used for the in situ analysis of individual cells at atmospheric pressure. Single cell ablation was achieved by delivering mid-IR laser pulses through the etched tip of a GeO_2-based glass fiber. Metabolic analysis was performed from single cells and small cell populations of *Allium cepa* and *Narcissus pseudonarcissus* bulb epidermis, as well as single eggs of *Lytechinus pictus*. Of the 332 peaks detected for *A. cepa*, 35 were assigned to metabolites with the help of accurate ion masses and tandem MS. The metabolic profiles from single cells of the two plant species included a large variety of oligosaccharides including possibly fructans in *A. cepa*, and alkaloids, e.g., lycorine in *N. pseudonarcissus*. Analysis of adjacent individual cells with a difference in pigmentation showed that, in addition to essential metabolites found in both variants, the pigmented cells contained anthocyanidins, other flavonoids, and their glucosides. Analysis of single epidermal cells from different scale leaves in an *A. cepa* bulb showed metabolic differences corresponding to their age. Our results indicate the feasibility of using LAESI-MS for the in situ analysis of metabolites in single cells with potential applications in studying cell differentiation, changes due to disease states, and response to xenobiotics.

Information on the chemical composition within a cell has implications in the understanding of cell metabolism, division, disease states, ecological effects, etc.[1,2] Cells of the same type exhibit diverse metabolic makeup depending on their phase in the cell cycle, history, and interaction with the environment. In vivo analysis of metabolites in a single cell is challenging because of the limited size and complexity of the sample. Spectrochemical analysis, such as Fourier transform-infrared (FT-IR) spectroscopic imaging,[3] coherent anti-Stokes Raman scattering (CARS) microscopy,[4] and nuclear magnetic resonance[5] have been utilized to explore the chemical makeup of a single cell. Most of the used techniques, however, require chemical tagging of the analyte by a fluorophore[6] or the genetic incorporation of green fluorescent protein (GFP)[7] and do not provide simultaneous detection of more than a few components.[8] The direct chemical analysis of a single cell by capillary electrophoresis (CE), performed, for example, by inserting a microcapillary into the cell, has broadened the variety of analyzed species.[9−12] Multiple components were de-

* Corresponding author. Phone: +1(202)994-2717. Fax: +1(202)994-5873. E-mail: vertes@gwu.edu.

(1) Kehr, J. *Curr. Opin. Plant Biol.* **2003**, *6*, 617–621.
(2) Monroe, E. B.; Jurchen, J. C.; Rubakhin, S. S.; Sweedler, J. V. In *New Frontiers in Ultrasensitive Bioanalysis: Advanced Analytical Chemistry Applications in Nanobiotechnology, Single Molecule Detection, and Single Cell Analysis* ; Xu, X.-H. N., Ed., Wiley-Interscience: Hoboken, NJ, 2007; pp 269−293.
(3) Malik, Z.; Dishi, M.; Garini, Y. *Photochem. Photobiol.* **1996**, *63*, 608–614.
(4) Potma, E. O.; De Boeij, W. P.; Van Haastert, P. J. M.; Wiersma, D. A. *Proc. Natl. Acad. Sci. U.S.A.* **2001**, *98*, 1577–1582.
(5) Aguayo, J. B.; Blackband, S. J.; Schoeniger, J.; Mattingly, M. A.; Hintermann, M. *Nature* **1986**, *322*, 190–191.
(6) Miyawaki, A.; Sawano, A.; Kogure, T. *Nat. Rev. Mol. Cell Biol.* **2003**, *4*, S1–S7.
(7) Tsien, R. Y. *Annu. Rev. Biochem.* **1998**, *67*, 509–544.
(8) Navratil, M.; Mabbott, G. A.; Arriaga, E. A. *Anal. Chem.* **2006**, *78*, 4005–4020.
(9) Kennedy, R. T.; Oates, M. D.; Cooper, B. R.; Nickerson, B.; Jorgenson, J. W. *Science* **1989**, *246*, 57–63.
(10) Olefirowicz, T. M.; Ewing, A. G. *Anal. Chem.* **1990**, *62*, 1872–1876.
(11) Hogan, B. L.; Yeung, E. S. *Anal. Chem.* **1992**, *64*, 2841–2845.
(12) Cruz, L.; Moroz, L. L.; Gillette, R.; Sweedler, J. V. *J. Neurochem.* **1997**, *69*, 110–115.

10.1021/ac901525g CCC: $40.75
Published on Web 09/17/2009

tected by coupling CE with electrospray ionization (ESI) mass spectrometry (MS).[13,14] Other mass spectrometric techniques, such as matrix-assisted laser desorption ionization (MALDI) and secondary ion mass spectrometry (SIMS), in a vacuum environment have demonstrated the analysis of vesicles and lipid membranes.[15,16] Most single cell analysis is performed in vitro on isolated cells or cell extracts[2,17,18] and aided by techniques such as laser capture microdissection to select a single cell for mass spectrometric analysis.[19] Current in situ MS methods, such as desorption ESI (DESI)[20,21] or atmospheric pressure infrared MALDI,[22,23] have been used to produce metabolic profiles from biological tissues averaged over cell populations.

Laser ablation electrospray ionization (LAESI) is a new ionization technique that uses a focused mid-IR laser beam with a wavelength of 2.94 μm to sample material directly from tissue based on the strong absorption of water at this wavelength.[24,25] In LAESI, the ablation plume, consisting mostly of neutrals, is intercepted by an electrospray to efficiently postionize its content. Focusing with conventional optics, e.g., using a single CaF_2 lens, results in a typical ablation diameter of 250 μm that is too large for most single cells. Although the diffraction limit for the ~3 μm light used in these studies is ~1.5 μm, lens aberrations and the long working distance necessary for interfacing with the mass spectrometer result in much larger spot sizes. As most plant and animal cells are in the 20−200 and 5−50 μm size range, respectively, single cell analysis by LAESI-MS requires infrared ablation on the 10−100 μm scale. LAESI-MS has demonstrated in situ analysis of metabolites and lipids from both plant and animal tissues.[24,26] A similar approach has been used to analyze carbohydrates and lipids of milk and egg yolk by infrared (IR) matrix-assisted laser desorption electrospray ionization (MALDESI).[27]

Here we show that metabolic profiles can be obtained by LAESI-MS from single cells and small cell populations of onion (*Allium cepa*) and daffodil (*Narcissus pseudonarcissus*) bulb epidermal cells. Comparison of the metabolic profiles from these two species reveals a variety of oligosaccharides including possibly fructans and anthocyanins in *A. cepa* and alkaloids, e.g., norpulviine, in *N. pseudonarcissus* cells. Analysis of adjacent cells with or without pigment in the epidermal tissue reveals significant differences in the metabolite content. Accurate mass measurement and structural information, obtained by tandem MS, enable the identification of numerous metabolites from a single cell. Comparing these profiles for cells of different type and of different environmental history provides insight into cellular development and response.

EXPERIMENTAL SECTION

Laser Ablation Electrospray Ionization. Mid-IR laser light was delivered to the target through a germanium oxide (GeO_2)-based optical fiber (450 μm core diameter, HP Fiber, Infrared Fiber Systems, Inc., Silver Spring, MD) with its tip etched to a 15 μm radius of curvature. Laser radiation was produced by a diode pumped Nd:YAG laser-driven optical parametric oscillator (OPO) (Opolette 100, Opotek, Carlsbad, CA) at 2940 nm, 100 Hz repetition rate, and 5 ns pulse width. The energy of a laser pulse before coupling into the optical fiber was 554 ± 26 μJ, thus the pulse-to-pulse energy stability corresponded to ~5%. The laser system was operated at 100 Hz for ~1 s to ablate a cell, thus, up to 100 laser shots were delivered to a cell for analysis. For the postionization of the ablated neutrals, 50% methanol with 0.1% (v/v) acetic acid was electrosprayed under a right angle into the ablation plume. In the home-built electrospray source, a low noise syringe pump (Physio 22, Harvard Apparatus, Holliston, MA) was used to supply the solution at 200 nL/min to a tapered stainless steel emitter (i.d. 50 μm, MT320-50-5-5, New Objective, Woburn, MA). A stable high voltage between 2.7 and 2.9 kV, generated by a regulated power supply (PS350, Stanford Research Systems, Sunnyvale, CA), was applied to the emitter, which was mounted on a manual translation stage for the optimization of the laser ablation electrospray ionization (LAESI) signal.

The mass spectrometer orifice was on the same axis as the electrospray emitter of the LAESI source at a distance of ~12 mm from the tip. The sample was placed on a precleaned microscope glass slide (catalog no. 125496, Fisher Scientific, Pittsburgh, PA) ~15 mm below the spray axis on a stepper motor-driven three-axis precision flexure stage (NanoMax TS, Thorlabs, Newton, NJ). Without the ESI on, no ions were detected by the mass spectrometer, indicating that no ions directly induced by the laser were collected. This was the result of the large (>15 mm) distance between the orifice of the mass spectrometer and the ablated sample.

The positive ions produced by the LAESI source were analyzed by an orthogonal acceleration time-of-flight mass spectrometer (Q-TOF Premier, Waters Co., MA) (see Figure 1) at a mass resolution of 8 000 (fwhm). The orifice of the mass spectrometer had an inner diameter of 127 μm. The interface block temperature was held at 80 °C, and its potential was kept at −70 V. Tandem mass spectra were obtained by collision activated dissociation (CAD) with argon as the collision gas at a typical collision cell pressure of 4×10^{-3} mbar and with collision energies between 10 and 25 eV.

Ablation Using Optical Fiber Tips. The laser beam was steered by gold-coated mirrors (PF10-03-M01, Thorlabs, Newton, NJ) and coupled into the cleaved end of the optical fiber by a 50 mm focal length plano-convex calcium fluoride lens (Infrared

(13) Hofstadler, S. A.; Severs, J. C.; Smith, R. D.; Swanek, F. D.; Ewing, A. G. *Rapid Commun. Mass Spectrom.* **1996**, *10*, 919–922.
(14) Tsuyama, N.; Mizuno, H.; Tokunaga, E.; Masujima, T. *Anal. Sci.* **2008**, *24*, 559–561.
(15) Rubakhin, S. S.; Garden, R. W.; Fuller, R. R.; Sweedler, J. V. *Nat. Biotechnol.* **2000**, *18*, 172–175.
(16) Ostrowski, S. G.; Van Bell, C. T.; Winograd, N.; Ewing, A. G. *Science* **2004**, *305*, 71–73.
(17) Stahl, B.; Linos, A.; Karas, M.; Hillenkamp, F.; Steup, M. *Anal. Biochem.* **1997**, *246*, 195–204.
(18) Amantonico, A.; Oh, J. Y.; Sobek, J.; Heinemann, M.; Zenobi, R. *Angew. Chem., Int. Ed.* **2008**, *47*, 5382–5385.
(19) Emmert-Buck, M. R.; Bonner, R. F.; Smith, P. D.; Chuaqui, R. F.; Zhuang, Z.; Goldstein, S. R.; Weiss, R. A.; Liotta, L. A. *Science* **1996**, *274*, 998–1001.
(20) Takats, Z.; Wiseman, J. M.; Gologan, B.; Cooks, R. G. *Science* **2004**, *306*, 471–473.
(21) Talaty, N.; Takats, Z.; Cooks, R. G. *Analyst* **2005**, *130*, 1624–1633.
(22) Li, Y.; Shrestha, B.; Vertes, A. *Anal. Chem.* **2007**, *79*, 523–532.
(23) Shrestha, B.; Li, Y.; Vertes, A. *Metabolomics* **2008**, *4*, 297–311.
(24) Nemes, P.; Vertes, A. *Anal. Chem.* **2007**, *79*, 8098–8106.
(25) Nemes, P.; Barton, A. A.; Li, Y.; Vertes, A. *Anal. Chem.* **2008**, *80*, 4575–4582.
(26) Sripadi, P.; Nazarian, J.; Hathout, Y.; Hoffman, E. P.; Vertes, A. *Metabolomics* **2009**, *5*, 263–276.
(27) Sampson, J. S.; Murray, K. K.; Muddiman, D. C. *J. Am. Soc. Mass Spectrom.* **2009**, *20*, 667–673.

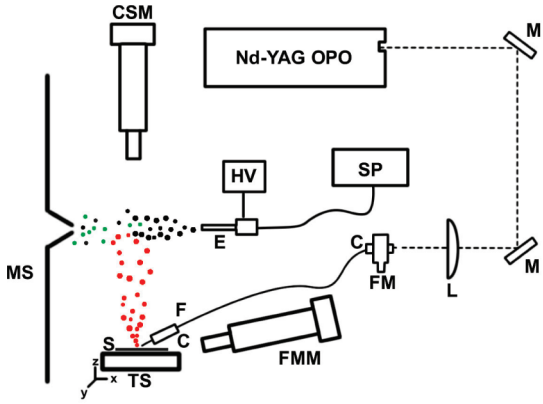

Figure 1. Schematics of instrumental setup for single cell analysis by LAESI-MS. The mid-IR ablation products (red dots) generated by the etched optical fiber tip (F) are intercepted by the electrospray plume (black dots) and postionized to form ions (green dots) sampled by the mass spectrometer (MS). A long-distance video microscope (fiber monitor, FMM) is utilized to maintain constant distance between the fiber tip and the sample surface (S). The sample is placed on a three-axis translation stage (TS), and a second video microscope (cell spotting microscope, CSM) is used to target the cells. The electrospray is produced by applying high voltage (HV) to the capillary emitter (E) and by maintaining a constant solution flow rate by a syringe pump (SP). Pulses from the mid-IR OPO are coupled to the optical fiber, adjusted by a fiber chuck (C) and a five-axis fiber mount (FM), using two Au-coated mirrors (M) and a CaF_2 lens (L).

Optical Products, Farmingdale, NY). The optical fiber, held by a bare fiber chuck (BFC300, Siskiyou Corporation, Grants Pass, OR), was positioned by a five-axis translator (BFT-5, Siskiyou Corporation, Grants Pass, OR).

The GeO_2-based glass fiber was used because of its high laser-damage threshold due to its high glass transition temperature.[28] After stripping off the Hytrel and the polyimide coatings on both ends of the fiber by the application of 1-methyl-2-pyrrolidinone (at 130 to 150 °C for ~1 min), the fiber ends were cleaved with a Sapphire blade (KITCO Fiber Optics, Virginia Beach, VA) by scoring and gently snapping them. Chemical etching of the fiber tip was achieved by dipping one of the cleaved fiber ends ~0.5 mm deep into 24 °C 1% HNO_3 solution in a wide beaker to provide a low meniscus curvature. The meniscus formed at the fiber end gradually etched the 450 μm diameter core into a sharp tip (see Figure 2a) with a radius of curvature $R \approx 15$ μm. Prior to use, the etched tips were washed with deionized water. No visible change of the fiber tip was observed after the LAESI experiments.

The etched end of the fiber was attached to a micromanipulator (MN-151, Narishige, Tokyo, Japan) and brought to close proximity of the sample. Alignment of the coordinate system so that the $x-y$ plane coincided with the sample and the x axis was parallel with the emitter, the optical fiber was positioned at azimuth and zenith angles of 135° and 45°, respectively. Following the LAESI signal as a function of the zenith angle, we determined that 45° provided an acceptable trade-off between the shape of the ablation mark and signal intensity reduction by blocking the expanding plume. In a few instances, after ablation a thin material deposit was observed on the fiber tip. In these cases, the fiber was

(28) Harrington, J. A. In *Specialty Optical Fibers Handbook*; Méndez, A., Morse, T. F., Eds.; Academic Press: Burlington, MA, 2007.

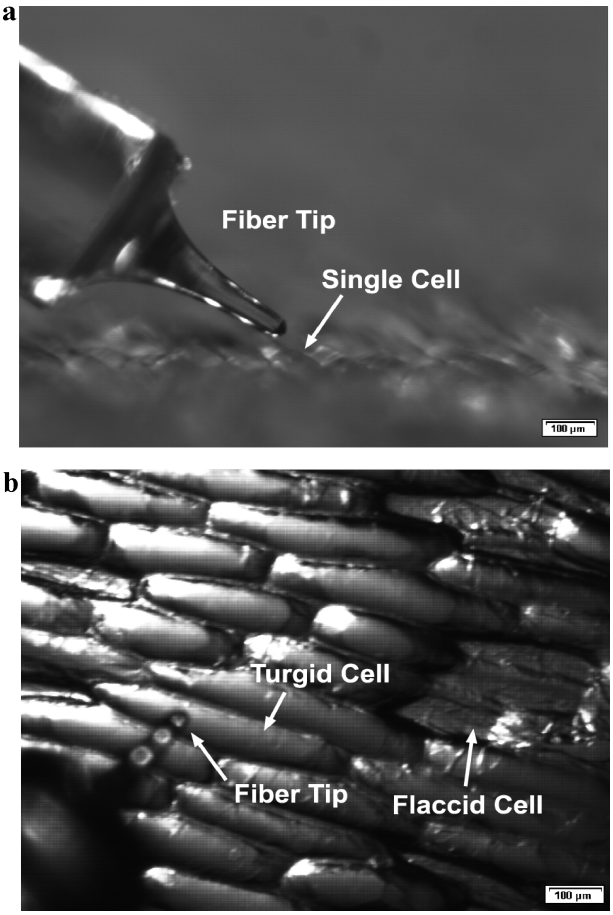

Figure 2. (a) Etched optical fiber tip and the raised surface of turgid epidermal cells of *A. cepa* were ~30 μm apart. For optimum coupling of the laser energy, this distance was similar to the diameter of the tip. Further removal of the fiber tip from the cell surface resulted in no ablation, whereas closer approach often led to damage to the cell or the fiber tip. (b) Cell targeting for ablation was carried out by adjusting the lateral position of the fiber tip over the selected turgid cell in the tissue. Scale bars are 100 μm.

retracted from the surface and elevated laser pulse energy was used to clean the tip. Usually, the distance between the fiber tip and the sample surface, h, was set close to $h \approx 2R$, resulting in an ablation mark with an average diameter $\langle D \rangle \approx 2.5R$. Microscope images of the ablation marks were obtained in either reflected or transmitted mode by an upright microscope (BX 51, Olympus America Inc., Center Valley, PA).

Visualization System. The distance between the fiber tip and sample surface was monitored by a long distance video microscope (InFocus Model KC, Infinity, Boulder CO) with a 5× infinity-corrected objective lens (M Plan Apo 5×, Mitutoyo Co., Kanagawa, Japan), and the image was captured by a CCD camera (Marlin F131, Allied Vision Technologies, Stadtroda, Germany). With the environmental vibration in the low micrometer range, an approximate distance of 30−40 μm was easily maintained between the tip and the selected cell. A similar video microscope system was used at a right angle to the sample surface to align the fiber tip over the cell of choice for ablation. This system consisted of a 7× precision zoom optic (Edmund Optics, Barrington, NJ), fitted with a 10× infinity-corrected long working distance objective lens (M Plan Apo 10×, Mitutoyo Co., Kanagawa, Japan) and a CCD

camera (Marlin F131, Allied Vision Technologies, Stadtroda, Germany).

Chemicals. HPLC grade methanol and water were purchased from Acros Organics (Geel, Belgium), and glacial acetic acid was obtained from Fluka (Munich, Germany). These chemicals were used without further purification.

Cells. Ten organic purple *A. cepa* bulbs (5−7 cm transverse diameter) were purchased from a local store (distributed by CFF Fresh, Sedro-Woolley, WA and bought in Washington, DC), and four *N. pseudonarcissus* bulb were obtained from Reston, VA. Prior to the experiments, the bulbs were stored at 4 °C. Before LAESI-MS analysis, the bulbs were cut longitudinally by a surgical scalpel. A layer of scale was selected and cut into a strip between 4 and 6 cm^2. The intact monolayer of the inner epidermal tissue from the concave surface was peeled away from the parenchyma tissue. The wet surface of the epidermis was used to mount the tissue to a glass slide for LAESI-MS analysis.

Unfertilized *Lytechinus pictus* (painted sea urchin) eggs were collected by injecting the animal with 0.5 M KCl solution. Prior to the LAESI-MS analysis, the eggs were stored in a refrigerator (4 °C) in artificial seawater. For the ablation experiments, a single egg was held by a holding micropipet (MPH-MED-O, Humagen Fertility Diagnostic, VA) mounted on a micromanipulator (NMN-21, Narishige International USA, Inc., NY). Suction was induced by a manual injector (IM-9A, Narishige International USA, Inc., NY).

Peak Assignments. Because of the diversity of structural isomers, assignments of the peaks to specific metabolites required special care. High mass resolution ($m/\Delta m \approx 8\,000$, fwhm) and mass accuracy (~1 mDa or ~5 ppm at m/z 200) helped to identify a selection of potential structures. The measured monoisotopic masses, m/z_{meas}, in Tables S1−S3 in the Supporting Information were obtained from a typical single cell spectrum, whereas the calculated values, m/z_{calc}, were derived using the NIST Isotope Calculator package (ISOFORM, version 1.02). The Plant Metabolic Network database (http://plantcyc.org/; last accessed on June 8, 2009) and species-specific literature[29,30] were also used as input for possible candidates. Tentative peak assignments were made based on the accurate masses, the isotope distribution patterns, and in some cases, the CAD spectra. Final identification of the ions requires additional work based on separation techniques, ultrahigh resolution MS, ^1H and ^{13}C NMR, and FT-IR.

Relative Quantitation. For solutions with only a few components, quantitation capabilities of LAESI-MS were demonstrated throughout a wide dynamic range.[24] For more complex biological tissue matrixes, relative quantitation was established.[26] For layer-by-layer comparison of relative metabolite abundances in individual cells, LAESI-MS was performed to analyze four cells for each of the studied layers. The spectra were normalized to the base peaks, and relative abundances and their standard deviations were calculated for the metabolites of interest.

RESULTS AND DISCUSSION

Laser Ablation of a Single Plant Cell. Smaller ablation craters can be produced by delivering the laser light through an optical fiber with an etched tip to reduce its diameter.[31] This approach to focusing is similar to the one applied in scanning near-field optical microscopy (SNOM), but in the current study, the produced spot size is still well above the diffraction limit. A GeO_2-based glass fiber with an etched tip with $R \approx 15$ μm radius of curvature was utilized to deliver the 2.94 μm wavelength infrared light. When placed in close proximity of the sample surface, the average diameter of the ablation mark, $\langle D \rangle$, was slightly larger than $2R$. Because an accidental contact between the tip and the cells could break the fiber tip or damage the cell wall, the distance between the fiber tip and sample surface was adjusted by a micromanipulator and a micropositioning stage with the help of a long distance microscope (see Figure 2a). A similar long distance microscope was used under a right angle to the tissue surface for cell targeting (see Figure 2b). With assumption of length, width, and depth dimensions of 300, 50, and 100 μm, respectively, the average volume of a large epidermal cell is ~1.5 nL, but the interaction volume is only ~30 pL for the 30−40 μm ablation spot diameter. Thus the fiber-based LAESI experiments probe only a fraction of these large cells. The schematic of the single cell LAESI-MS system is shown in Figure 1.

Large epidermal cells from the *A. cepa* bulb, a model system to study plant cell structures,[32] and from the *N. pseudonarcissus* bulb were used to demonstrate single cell analysis by LAESI-MS. In this tissue, the potential cross-contamination induced by the analysis of neighboring cells in the same layer was negligible because of the large cell size. Because of the monolayer structure, there was no mixing from the underlying tissue either. Perforation marks produced by mid-IR ablation on single turgid epidermal cells of the two samples are shown in parts a and c of Figure 3. These marks indicated the sampling of the selected individual cells, with no visible effect on the neighboring regions. Ablation typically started at the second laser pulse and continued until all the cytoplasm has been ablated and/or leaked out of the cell. Mass spectra were observed starting from the second laser pulse, as well. In the case of an *A. cepa* epidermal cell, after ~100 laser pulses no additional ablation took place.

There was a remarkable difference between ablating turgid cells and flaccid ones that had lost their cytoplasm. The ablation marked A in Figure 3a shows a relatively large opening corresponding to the turgid state, whereas the smaller hole in the same cell wall was produced in a flaccid state after the cytoplasm had been removed. It is important to emphasize that in the case of every intact cell, ablation was successfully carried out. The larger size of the ablation marked A in Figure 3a and the ruptured cell wall indicate the explosive nature of cytoplasm sampling in the turgid state. The presence of rapid phase explosion in the ablation of water-rich targets has been demonstrated by modeling studies.[33] In the flaccid state (i.e., in the absence of cytoplasm), however, sampling of the cell wall only is indicated by the smaller opening.

(29) Bastida, J.; Viladomat, F.; Codina, C. In *Studies in Natural Products Chemistry*; Rahman, A.-u., Ed.; Elsevier Science B. V.: Amsterdam, The Netherlands, 1998; Vol. 20, pp 323−405.
(30) Slimestad, R.; Fossen, T.; Vagen, I. M. *J. Agric. Food Chem.* **2007**, *55*, 10067–10080.
(31) Stockle, R.; Setz, P.; Deckert, V.; Lippert, T.; Wokaun, A.; Zenobi, R. *Anal. Chem.* **2001**, *73*, 1399–1402.
(32) Wilson, R. H.; Smith, A. C.; Kacurakova, M.; Saunders, P. K.; Wellner, N.; Waldron, K. W. *Plant Physiol.* **2000**, *124*, 397–406.
(33) Chen, Z. Y.; Vertes, A. *Phys. Rev. E* **2008**, *77*, 036316.

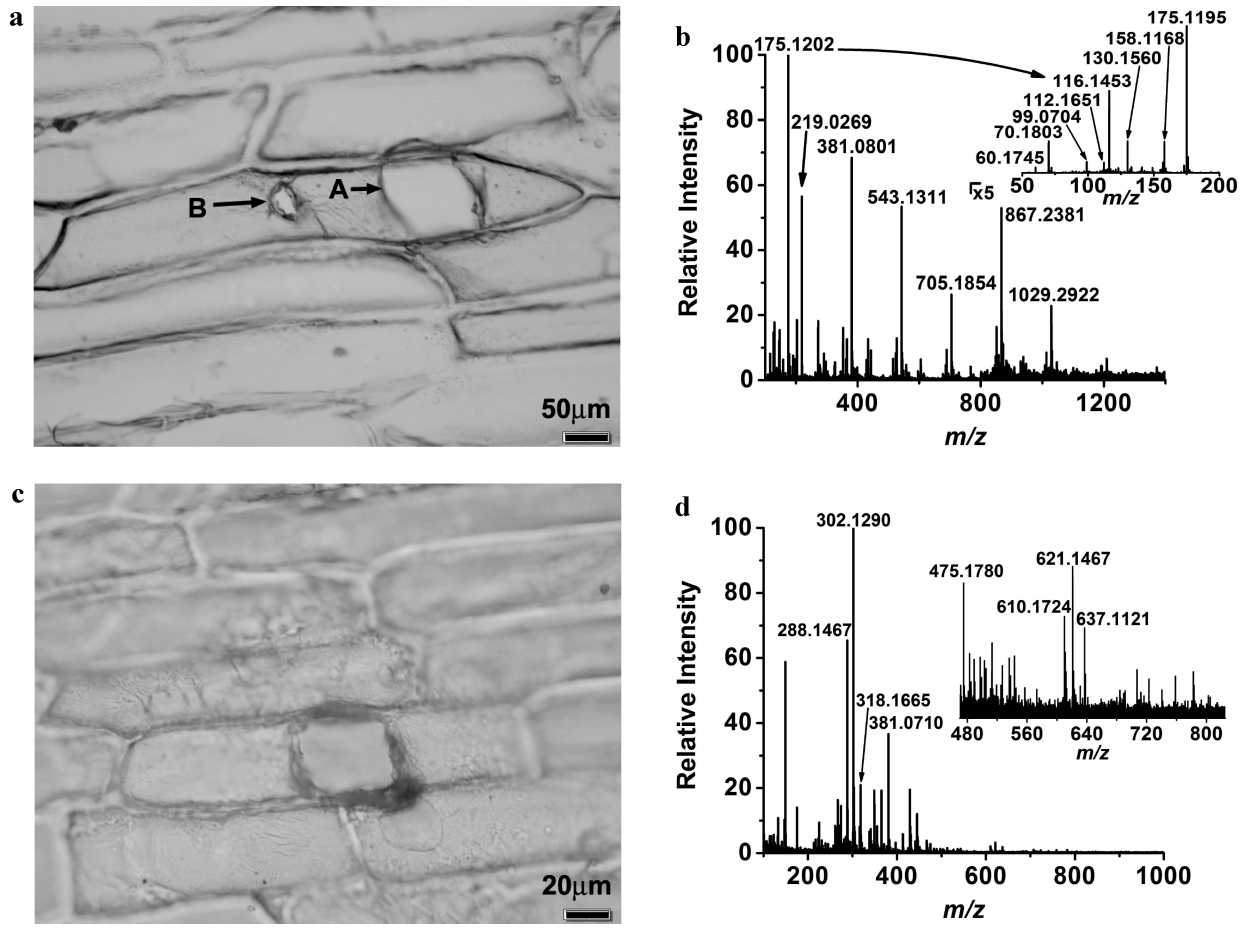

Figure 3. Single cell ablation marks on epidermal cell of (a) *A. cepa* (unpigmented cell) and (c) *N. pseudonarcissus* produced through an etched optical fiber tip. In panel a, the first ablation (marked A) was performed on a turgid cell, whereas the second ablation (marked B) occurred after the loss of cytoplasm when the cell became flaccid. Panels b and d show the corresponding LAESI mass spectra produced by 100 laser pulses for *A. cepa* and *N. pseudonarcissus*, respectively. The inset in panel b depicts the eight fragments in the tandem MS of the nominal *m*/*z* 175 ion produced by CAD. The inset in panel d shows the zoomed portion of the daffodil spectrum at higher *m*/*z*.

Laser Ablation of a Single Animal Cell. Individual eggs of *L. pictus* (painted sea urchin) were analyzed in sessile configuration. A few minutes before the LAESI-MS analysis, 30 μL of the *L. pictus* egg suspension was mixed with 1 mL of water to decrease the number of eggs per unit volume. This increased the average distance between the eggs and enabled their individual manipulation. Furthermore, the dilution reduced the concentration of salts. This was necessary because the high salt concentration prevented the detection of metabolite ions. Approximately 100 μL of the resulting egg suspension was placed on a glass slide. A single egg of 90 to 100 μm in diameter was selected and immobilized by a holding pipet using suction induced by a manual injector. The pipet was positioned by a micromanipulator. The ablation for LAESI-MS was carried out by moving the etched fiber tip to contact the *L. pictus* egg (see the inset of Figure 4). In order to initiate ablation, slightly more efficient coupling of the laser pulse to the optical fiber was achieved, which in relative terms translated into somewhat higher laser fluences at the sharpened fiber tip compared to the epidermal cells.

Figure 4 shows the LAESI mass spectrum acquired from a single egg. The preliminary analysis of the data shows the presence of ions representing small metabolites along with lipids at higher masses. Some of the prominent ions include species at nominal *m*/*z* 83, 101, 105, 115, 119, 138, 158, 217, 243, 261, 413, 625, and 755. Further work, including tandem MS, is needed to identify the corresponding metabolites.

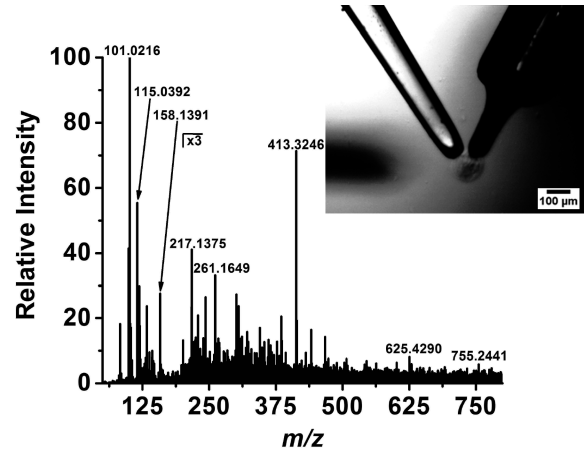

Figure 4. Positive ion LAESI mass spectrum of a single sea urchin (*L. pictus*) egg of ~100 μm in diameter. The inset shows the sessile egg immobilized by the holding pipet and touched by the sharpened optical fiber.

LAESI-MS and MS/MS from a Cell. LAESI mass spectra were only produced from turgid cells. Except in the case of *N. pseudonarcissus*, all the tandem MS data were collected from the

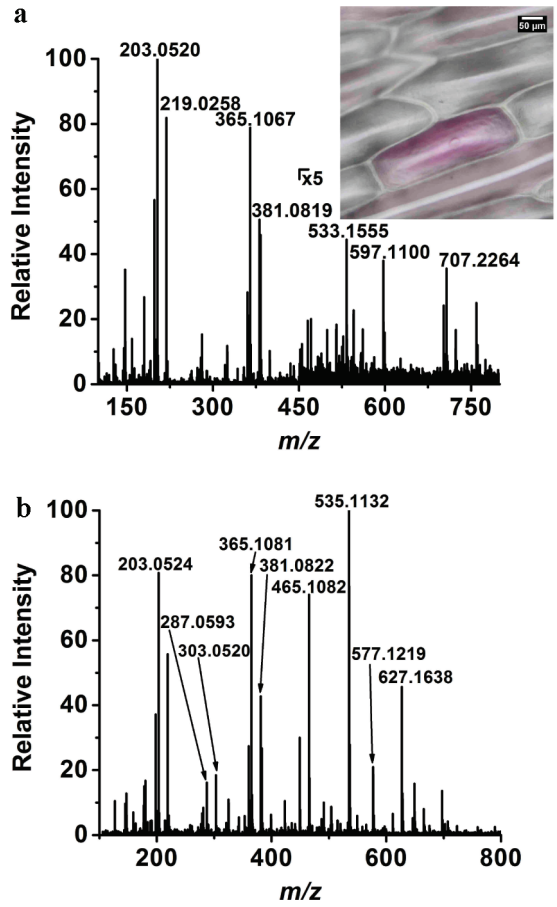

Figure 5. Single cell LAESI mass spectra of neighboring (a) colorless and (b) pigmented epidermal cells of the purple *A. cepa* cultivar with the optical image of the cells in the inset (scale bar = 50 μm).

single cells using up to a 100 laser pulses. Initially single cell spectra were combined to increase the signal-to-noise ratio and enhance the fidelity of peak assignments. The combined positive ion spectra from a population of 13 cells showed 332 peaks with a wide dynamic range. Once the assignments were made, single cell spectra were studied. Parts b and d of Figure 3 give examples of single cell mass spectra from the two plant species. Many of the ions were tentatively identified as primary or secondary metabolites based on accurate masses, isotope distribution patterns, and in some cases, tandem MS. In the onion cell, most of the singly charged low m/z ions ($<m/z$ 300) were assigned to smaller metabolites, such as alliin, 2-aminoacrylic acid, and thioacrolein found in the alliin degradation cycle. Most of the larger ions corresponded to secondary metabolites and oligosaccharides, possibly fructans, found in the fructan biosynthesis cycle. A number of doubly charged ions were also observed for oligosaccharides, which helped their identification up to a degree of polymerization of ten.

Some ions can have multiple assignments. For example, the m/z 175.1202 ion in the *A. cepa* spectrum can be assigned to arginine, acetyl-ornithine, *N*-methyltryptamine, and/or gramine. It was identified as protonated arginine based on better than 0.001 Da mass accuracy and comparing its CAD fragmentation pattern (see the inset in Figure 3b) to the corresponding tandem MS spectrum in the NIST Mass Spectral Search Program (NIST/EPA/NIH Mass Spectral Library, version 2.0). The ability of performing tandem MS on a single cell in situ has promising implications for ion identification in organisms.

To facilitate the data analysis and the peak assignments, averaged LAESI mass spectra were also taken on small cell populations using conventional focusing optics with ~250 μm focal spot size. As expected, these spectra showed higher S/N than the single cell data. Even with this additional information, because of the large variety of structural isomers, caution is necessary in making metabolite assignments.[29] Unambiguous identification of individual metabolites requires extensive studies relying on multiple methods, e.g., separation techniques, ultrahigh-resolution MS, ^{1}H and ^{13}C NMR, and FT-IR.

Metabolites from the Same Cell Type in Different Species. The analysis of the anatomically similar single epidermal cells from the two storage organs showed significantly different metabolic profiles. While the cells from both plants contained oligosaccharides, these species were more prevalent in the onion. The daffodil cells, however, were rich in various alkaloids, such as norpluviine, a lycorine type, and vittatine, a hemeanthamine type alkaloid. These and other *Narcissus* alkaloids are known to be present in this plant species.[29] The lists of peak assignments and mass accuracies for both species are presented in Tables S1 (*A. cepa*) and S2 (*N. pseudonarcissus*) of the Supporting Information.

Adjacent Colorless and Pigmented Cells. A fraction of the epidermal cells in the purple onion cultivar are pigmented and can be distinguished under the microscope. The presence of this cell variant enabled a direct comparison between the metabolite composition of the colorless and pigmented cells in the same tissue. In Figure 5, the corresponding mass spectra are presented together with the optical image of the two cell types.

Comparison of the LAESI mass spectra revealed that, in addition to the essential metabolites found in the colorless cells, the pigmented variant contained significant amounts of anthocyanidins, other flavonoids, and their glucosides. For example, the

Table 1. Relative Ion Intensities for Some Metabolites in Single Cells of an *A. cepa* Bulb Averaged for Four Cells

	leaf bases				
metabolites	fourth (inner)	fifth	sixth	seventh	eighth (outer)
arginine	97 ± 5	74 ± 28	6 ± 3	0	0
alliin	9 ± 4	11 ± 2	20 ± 7	19 ± 7	20 ± 3
monosaccharide	47 ± 11	60 ± 30	23 ± 13	40 ± 14	41 ± 51
disaccharide	87 ± 19	96 ± 7	72 ± 13	70 ± 7	77 ± 35
trisaccharide	78 ± 18	85 ± 13	100 ± 0	100 ± 0	48 ± 36
tetrasaccharide	47 ± 13	56 ± 8	80 ± 17	74 ± 11	20 ± 15
pentasaccharide	20 ± 8	27 ± 5	31 ± 7	25 ± 2	7 ± 6
hexasaccharide	6 ± 3	11 ± 2	10 ± 2	7 ± 2	1 ± 0
heptasaccharide	2 ± 2	4 ± 1	3 ± 0	1 ± 1	0

m/z 449 ion can be assigned to cyanidin glucoside, a known purple pigment contained in the cell membrane vacuoles in purple plants. A comparative list of the ions and the tentative metabolite assignments for the colorless and the pigmented cell are listed in Table S3 in the Supporting Information. Close to 70 ionic species were found in single cells. Two thirds of them were tentatively assigned to one or more metabolites that had accurate masses close to the measured values and for some of them the tandem MS that was consistent with known fragmentation patterns. The most significant difference between the colorless and pigmented cells was the presence of anthocyanins and the corresponding anthocyanidins in the latter. Glycosidic flavonoids had been detected by vacuum IR laser MS studies in red rose leaf tissues.[34] In addition, the pigmented cells contained high levels of quercetin and its mono-, di-, and triglucosides. The elevated presence of quercetin in purple or red onion bulbs is well documented.[30] The observation that the metabolites in colorless cells were not contaminated by anthocyanidins and anthocyanins from adjacent pigmented cells points to no or minimal damage of the neighboring cells by the ablation.

Metabolites in Cells of Different Age. To find metabolic changes primarily correlated with age for the same type of cells, we compared the epidermal cells from different leaf bases (layers) within individual onion bulbs, where the different layers represented older and younger cell populations.[35] The relative quantitation capabilities of LAESI-MS in a wide dynamic range had been shown in previous publications.[24,26] The relative ion intensities of some metabolites averaged for four cells per layer ($n = 4$) are shown in Table 1. Changes from the younger inner leaf base (layer four) to the oldest outer turgid layer (layer eight) illustrate the variations of the related metabolite content. For example, reduced arginine content can be seen in the older cell populations from the gradual drop in its relative ion intensity from 97 ± 5 (layer 4) to 0 (layer 7). Conversely, alliin seems to accumulate more in the cells of the outer layers.

CONCLUSIONS

We have shown that in situ metabolic analysis of single cells is possible by a modified version of LAESI-MS. With the use of a sharpened optical fiber tip, individual cells were ablated for analysis. Comparisons of cells with different pigmentation or age within the same tissue as well as between cells of the same type in different species demonstrated significant metabolic variations consistent with literature data.

Laser based atmospheric pressure mass spectrometric techniques, such as LAESI-MS, are able to analyze small sample volumes with a tightly focused laser beam. Further developments in single cell analysis should focus on reducing the ablation spot size while maintaining the mass spectrometric signal by optimizing the source geometry and increasing the postionization yield. In heterogeneous cell populations, automatic adjustment of the laser parameters based on optical feedback can facilitate the analysis of multilayered populations cell by cell. An important future extension of this method is the analysis of biological tissues, with the ultimate goal of molecular imaging based on cells as the natural voxels. Metabolic analysis of single cells helps to better understand cell differentiation, aging, changes due to disease states, and response to xenobiotics and physical stimuli.

(34) Dreisewerd, K.; Draude, F.; Kruppe, S.; Rohlfing, A.; Berkenkamp, S.; Pohlentz, G. *Anal. Chem.* **2007**, *79*, 4514–4520.
(35) Darbyshire, B.; Henry, R. J. *New Phytol.* **1978**, *81*, 29–34.

ACKNOWLEDGMENT

The authors acknowledge financial support from the U.S. National Science Foundation (Grant 0719232), the U.S. Department of Energy (Grant DEFG02-01ER15129), the W. M. Keck Foundation (Grant 041904), and the George Washington University Research Enhancement Fund. Infrared Fiber Systems, Silver Spring, MD, generously provided the GeO_2-based glass optical fibers for this study, and Mark E. Reeves and Joan A. Hoffmann of George Washington University (GWU) helped with the protocol regarding their etching. The sea urchin eggs were kindly supplied by Kenneth M. Brown of GWU.

SUPPORTING INFORMATION AVAILABLE

Additional information as noted in text. This material is available free of charge via the Internet at http://pubs.acs.org.

Received for review July 9, 2009. Accepted September 8, 2009.

AC901525G

Supporting Information for

In Situ Metabolic Profiling of Single Cells by Laser Ablation Electrospray Ionization Mass Spectrometry

*Bindesh Shrestha and Akos Vertes**

Department of Chemistry, W. M. Keck Institute for Proteomics Technology and Applications, The George Washington University, Washington, DC 20052

* Corresponding author. Phone: +1(202)994-2717, Fax: +1(202)994-5873, Email: vertes@gwu.edu

Table S1. Tentative peak assignments in the mass spectrum of a single unpigmented epidermal cell from *A. cepa* bulb.

Metabolites	**Formula**	$m/z_{\text{calc.}}$	$m/z_{\text{meas.}}$	**Δm (mDa)**
pyruvaldehyde	$C_3H_4O_2$ $(+H^+)$	73.0290	73.0188	-10.2
thioacrolein	C_3H_4S $(+H^+)$	73.0112	73.0188	7.6
5-aminoimidazole	$C_3H_5N_3$ $(+H^+)$	84.0562	84.0452	-11.0
furanone	$C_4H_4O_2$ $(+H^+)$	85.0290	85.0310	2.0
2-aminoacrylic acid	$C_3H_5NO_2$ $(+H^+)$	88.0399	88.0426	2.7
proline	$C_5H_9NO_2$ $(+H^+)$	116.0712	116.0747	3.5
2-oxohexa-4,5-cyclopropyl-5-enoic acid	$C_6H_6O_3$ $(+H^+)$	127.0395	127.0440	4.5
thymine	$C_5H_6N_2O_2$ $(+H^+)$	127.0508	127.0440	-6.8
5-oxoproline	$C_5H_7NO_3$ $(+H^+)$	130.0504	130.0527	2.3
p-aminobenzoic acid and/or vitamin L1	$C_7H_7NO_2$ $(+H^+)$	138.0555	138.0493	-6.2
glutamine and/or 3-ureido-isobutyric acid	$C_5H_{10}N_2O_3$ $(+H^+)$	147.0770	147.0811	4.1
histidine and/or bacimethrin	$C_6H_9N_3O_2$ $(+H^+)$	156.0773	156.0833	6.0
allylcysteine	$C_6H_{11}NO_2S$ $(+H^+)$	162.0589	162.0678	8.9
acetylhomoserine, α-aminoadipic acid	$C_6H_{11}NO_4$ $(+H^+)$	162.0766	162.0678	-8.8
phenylalanine	$C_9H_{11}NO_2$ $(+H^+)$	166.0868	166.0914	4.6
arginine [b]	$C_6H_{14}N_4O_2$ $(+H^+)$	175.1195	175.1202	0.7
alliin	$C_6H_{11}NO_3S$ $(+H^+)$	178.0538	178.0606	6.8
galactosamine	$C_6H_{13}NO_5$ $(+H^+)$	180.0872	180.0815	-5.7
tyrosine and/or α-aminooxy-β-phenylpropionic acid	$C_9H_{11}NO_3$ $(+H^+)$	182.0817	182.0807	-1.0
monosaccharide [a]	$C_6H_{12}O_6$ $(+K^+)$	219.0271	219.0269	-0.2
arginino-succinic acid	$C_{10}H_{18}N_4O_6$ $(+H^+)$	291.1305	291.1224	-8.1
glucosan or dextrin unit	$(C_6H_{10}O_5)_2$ $(+H^+)$ [c]	325.1135	325.1068	-6.7
disaccharide [a,b]	$C_{12}H_{22}O_{11}$ $(+K^+)$	381.0799	381.0801	0.2
trisaccharide [a,b]	$C_{18}H_{32}O_{16}$ $(+K^+)$	543.1328	543.1311	-1.7
heptasaccharide [a]	$C_{42}H_{72}O_{36}$ $(+H^+ + K^+)$	596.1759	596.1743	-1.6
oligosaccharide (DP 8 units) [a, c]	$C_{48}H_{82}O_{41}$ $(+H_2O + H^+ + K^+)$	686.2076	686.2177	10.1
tetrasaccharide [a,b]	$C_{24}H_{42}O_{21}$ $(+K^+)$	705.1856	705.1854	-0.2
oligosaccharide (DP 9 units) [a, c]	$C_{54}H_{92}O_{46}$ $(+H_2O + H^+ + K^+)$	767.2340	767.2286	-5.4
oligosaccharide (DP 10 units) [a, c]	$C_{60}H_{102}O_{51}$ $(+H_2O + H^+ + K^+)$	848.2604	848.2584	-2.0
pentasaccharide [a]	$C_{30}H_{52}O_{26}$ $(+K^+)$	867.2384	867.2381	-0.3
hexasaccharide [a, b]	$C_{36}H_{62}O_{31}$ $(+K^+)$	1029.2913	1029.2922	0.9

[a]Other adduct, and/or quasi-molecular, and/or cluster ions of the chemical species were also observed in the LAESI mass spectra.

[b]These ions were used as internal mass standards.

[c]DP = Degree of polymerization.

Table S2. Tentative peak assignments in the mass spectrum of a single epidermal cell from *N. pseudonarcissus* bulb.

Metabolites	Formula	$m/z_{calc.}$	$m/z_{meas.}$	Δm (mDa)
5-aminoimidazole	$C_3H_5N_3$ ($+H^+$)	84.0562	84.0468	-9.4
furanone	$C_4H_4O_2$ ($+H^+$)	85.0290	85.0295	0.5
proline	$C_5H_9NO_2$ ($+H^+$)	116.0712	116.0725	1.3
succinic acid	$C_4H_6O_4$ ($+H^+$)	119.0344	119.0243	-10.1
homoserine	$C_4H_9NO_3$ ($+H^+$)	120.0661	120.0809	14.8
3-methylene-indolenine	$C_5H_7NO_3$ ($+H^+$)	130.0504	130.0548	4.4
asparagine	$C_4H_8N_2O_3$ ($+H^+$)	133.0613	133.0638	2.5
glutamine and/or 3-ureido-isobutyric acid	$C_5H_{10}N_2O_3$ ($+H^+$)	147.0770	147.0799	2.9
histidine and/or bacimethrin	$C_6H_9N_3O_2$ ($+H^+$)	156.0773	156.0804	3.1
gallic acid	$C_7H_6O_5$ ($+H^+$)	171.0293	171.0203	-9
arginine [b]	$C_6H_{14}N_4O_2$ ($+H^+$)	175.1195	175.1218	2.3
caranine and/or crinine and/or vittatine	$C_{16}H_{17}NO_3$ ($+H^+$)	272.1287	272.1302	1.5
norpluviine	$C_{16}H_{19}NO_3$ ($+H^+$)	274.1443	274.1423	-2
galanthamine and/or mesembrenone and/or pluviine	$C_{17}H_{21}NO_3$ ($+H^+$)	288.1600	288.1467	-13.3
crinamine and/or haemanthamine	$C_{17}H_{19}NO_4$ ($+H^+$)	302.1392	302.1290	-10.2
homolycorine	$C_{18}H_{21}NO_4$ ($+H^+$)	316.1549	316.1512	-3.7
galanthine and/or lycorenine and/or papyramine	$C_{18}H_{23}NO_4$ ($+H^+$)	318.1705	318.1665	-4
disaccharides [a, b]	$C_{12}H_{22}O_{11}$ ($+K^+$)	381.0799	381.0710	-8.9
trisaccharides [a, b]	$C_{18}H_{32}O_{16}$ ($+K^+$)	543.1328	543.1394	6.6
tetrasaccharide	$C_{24}H_{42}O_{21}$ ($+H_2O+K^+$)	723.1961	723.1855	-10.6

[a]Other adduct, and/or quasi-molecular, and/or cluster ions of the chemical species were also observed in the LAESI mass spectra.

[b]These ions were used as internal mass standards.

Table S3. Comparative list of tentative peak assignments for the LAESI mass spectra of the colorless and pigmented cells in the onion bulb epidermis. The purple background in the table indicates ions found exclusively in the pigmented cells.

Metabolites	Formula	Purple	Colorless
furanone	$C_4H_4O_2$ ($+H^+$)	85.0268	85.0262
2-aminoacrylic acid	$C_3H_5NO_2$ ($+H^+$)	88.0388	88.0370
thymine and/or 2-oxohexa-4,5-cyclopropyl-5-enoic acid	$C_5H_6N_2O_2$ ($+H^+$) and/or $C_6H_6O_3$ ($+H^+$)	127.0374	127.0370
oxoproline	$C_5H_7NO_3$ ($+H^+$)	130.0546	130.0469
glutamine and/or 3-ureido-isobutyric acid	$C_5H_{10}N_2O_3$ ($+H^+$)	147.0766	147.0753
alliin	$C_6H_{11}NO_3S$ ($+H^+$)	178.0515	178.0525
galactosamine	$C_6H_{13}NO_5$ ($+H^+$)	180.0869	180.0870
monosaccharide [a]	$C_6H_{12}O_6$ ($+K^+$)	219.0259	219.0258
cyanidin and/or kaempferol	$C_{15}H_{11}O_6^+$	287.0593	-
quercetin	$C_{15}H_{10}O_7$ ($+H^+$)	303.0520	-
glucosan and/or dextrin unit [a]	$(C_6H_{10}O_5)_2$ ($+H^+$)	325.1122	325.1128
disaccharide [a]	$C_{12}H_{22}O_{11}$ ($+K^+$)	381.0822	381.0819
dityrosine	$C_{18}H_{20}N_2O_6$ ($+Na^+$)	383.1148	383.1148
disaccharide + quercetin glucoside	$C_{12}H_{22}O_{11}$ ($+K^+$) + $C_{21}H_{20}O_{12}$ ($+H^+$)	423.0884	-
cyanidin glucoside and/or kaempferol glucoside [a]	$C_{21}H_{21}O_{11}^+$	449.1164	-
peonidin glucoside	$C_{22}H_{23}O_{11}^+$	463.1262	-
quercetin glucoside [a]	$C_{21}H_{20}O_{12}$ ($+H^+$)	465.1082	
adenylyl aminoadipic acid	$C_{16}H_{23}N_6O_{10}P$ ($+H^+$)	491.1235	-
trisaccharide + quercetin glucoside	$C_{18}H_{32}O_{16}$($+K^+$) + $C_{21}H_{20}O_{12}$ ($+H^+$)	504.1145	-
cyanidin malonyl glucoside	$C_{24}H_{23}O_{14}^+$	535.1132	-
peonidin malonoyl glucoside	$C_{25}H_{25}O_{14}^+$	549.1303	-
trisaccharide	$C_{18}H_{32}O_{16}$ ($+H_2O+K^+$)	-	561.1495
cyanidin malonoyl acetoyl glucoside	$C_{26}H_{25}O_{15}^+$	577.1219	-
quercetin rutinoside, quercetin glucoside rhamnoside	$C_{27}H_{30}O_{16}$ ($+H^+$)	611.1697	-
cyanin, cyanidin diglucoside	$C_{27}H_{31}O_{16}^+$	611.1697	-
quercetin diglucoside [a]	$C_{27}H_{30}O_{17}$ ($+H^+$)	627.1638	-
cyanidin malonyl diglucoside	$C_{30}H_{33}O_{19}^+$	697.1754	-
tetrasaccharide	$C_{24}H_{42}O_{21}$ ($+H_2O+K^+$)	723.1995	723.2080
peonidin glucoside + quercetin	$C_{22}H_{23}O_{11}^+ + C_{15}H_{10}O_7$	765.1505	-
quercetin triglucoside	$C_{33}H_{40}O_{22}$ ($+H^+$)	789.2043	-
2 disaccharides + quercetin glucoside [a]	$C_{12}H_{22}O_{11} + C_{21}H_{20}O_{12}$ ($+Na^+$)	829.2299	-
2 disaccharides + quercetin diglucoside	$C_{12}H_{22}O_{11} + C_{27}H_{30}O_{17}$ ($+Na^+$)	991.2538	-
quercetin triglucoside + quercetin glucoside	$C_{33}H_{40}O_{22} + C_{21}H_{20}O_{12}$ ($+H^+$)	1253.3040	-
quercetin diglucoside + quercetin diglucoside [a]	$(C_{27}H_{30}O_{17})_2$ ($+H^+$)	1253.3040	-

[a]Other adduct, and/or quasi-molecular, and/or cluster ions of the chemical species were also observed in the LAESI mass spectra.